Shelled-isolated nanoparticle-enhanced Raman spectroscopy

Jian Feng Li, Yi Fan Huang, Yong Ding, Song Bo Li, Zhi Lin Yang, Xiao Shun Zhou, Feng Ru Fan,

Wei Zhang, Zhi You Zhou, De Yin Wu, Bin Ren, Zhong Lin Wang,* Zhong Qun Tian*

S1. Supplementary Methods

S1.1. Preparation of Au@SiO$_2$ core-shell NPs

We first synthesized Au NPs with a diameter of about 55 nm as cores by a standard sodium citrate reduction method.[1] A freshly prepared aqueous solution of 1 mM (3-Aminopropyl) trimethoxysilane (APS) was added to the gold sol under vigorous magnetic stirring in 15 min, ensuring complete complexation of the amine groups with the gold surface. Then a 0.54 wt% sodium silicate solution was added to the sol, again under vigorous magnetic stirring. To accelerate the synthesis procedure and make the ultra-thin silica shell, we elevated the reaction temperature from room temperature to 90 °C, so that the original coating time of 2-3 days[2] for coating silica shells of 4-5 nm can be shortened to ca. one hour. More importantly, this method ensures to form the ultra-thin shell thickness of only 2-4 nm that is free of pinholes (see S8) by carefully controlling parameters such as reaction time, temperature, pH, and the concentration.[2-7]

S1.2. Preparation of Au@Al$_2$O$_3$ core-shell NPs

The Au@Al$_2$O$_3$ core-shell NPs were prepared mainly by atomic layer deposition (ALD) technique[8].

Firstly, the cleaned and concentrated 55 nm Au NPs were spread over a cleaned glass. Then the ALD

was performed in a Savannah 100 Atomic Layer Deposition system manufactured by Cambridge

NanoTech Inc. During the deposition, the thickness of the Al_2O_3 layer could be controlled very well by

varying the number of cycles of deposition, where the growth rate was 0.1 nm per cycle. With such a

high precision of control, the Al_2O_3 layer covers the entire Au NPs uniformly.

S1.3. Methods for characterizing the core-shell nanoparticles

The structure and surface morphology of the core-shell nanoparticles and the shell thicknesses were

measured by high-resolution transmission electron microscopy (HRTEM) (JEM 4000EX and Tecnai

F30). Extinction spectra of 55 nm Au@SiO_2 sol with different silica shell thickness from 1 to 12 nm

were recorded on a Shimadzu UV-2100 spectrometer using a 1-cm quartz cell. After several rounds of

cleaning and concentrating by centrifugation, Au@SiO_2 NPs were spread onto the samples. The

electrochemical measurements were conducted in a conventional three-compartment glass cell on a

CHI 631B electrochemical workstation (CH Instruments, Shanghai, China). Raman spectra were

recorded on a LabRam I confocal microprobe Raman system (Jobin-Yvon, France) in a homemade

spectroelectrochemical cell. The excitation line was 632.8 nm from a He-Ne laser. The portable

Raman spectrometer (Inspetor, DeltaNu, USA) and the excitation line of 785 nm were used.

S1.4. Extinction spectra of Au@SiO_2 NPs

The extinction spectral features of 55 nm Au@SiO_2 sol with different silica shell thicknesses from 1

to 12 nm shown in Fig. S1a are quite similar to that of 55 nm Au NPs with a slight shift to the red,

indicating the effect of the shell on the localized surface plasmon resonances (LSPR) is negligible. It

should be noted that, in the SHINERS experiments, the particles are spread as a monolayer over the

substrate, the coupling effect between the nanoparticles themselves or between the particle and the

substrate can lead to a significant red-shift of the LSPR peak. We have performed a calculation based

on the generalized Mie theory. Because of the limitation of the calculation time, we have to use a large

Au NP (d = 200 nm) to simulate the much larger surface. As shown in Fig. S1b that the corresponding

peak is shifted from 540 nm to about 615 nm. Therefore, it is suitable to use the excitation line of 633

nm in the present study.
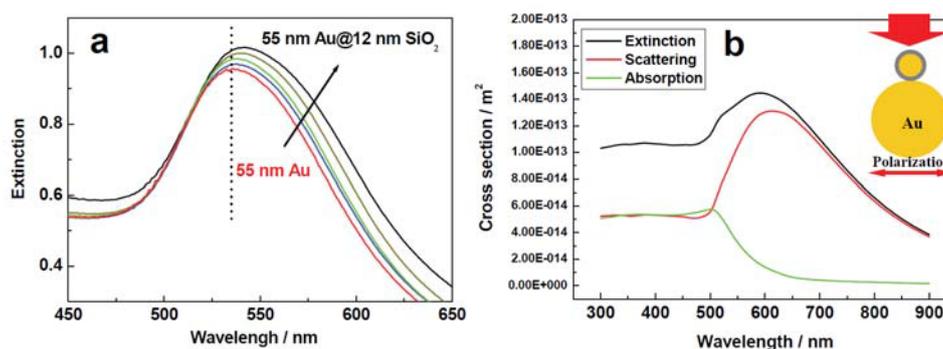
Figure S1 | The experimental and calculated extinction spectra. a, Extinction spectra of 55 nm Au@SiO_2 NPs with

different silica shell thicknesses from about 1 nm, 2 nm, 4 nm up to 12 nm in comparison with that of bare 55 nm Au

NPs. **b,** The Mie theory calculated extinction, absorption and scattering cross section of 55 nm Au@4 nm SiO_2 NP

contacting to Au NP of 200 nm in diameter.

S2. A previous strategy of using core-shell nanoparticles for extending the substrate generality

for SERS

Since the surface-enhanced Raman scattering (SERS) effect was discovered in the mid-1970s, most studies have been limited to Au, Ag and Cu substrates because these free-electron-like metals have appropriate values of the dielectric constant to fully support the effective electron oscillation, also known as the localized surface plasmon resonance (LSPR), which generates a large electromagnetic field near the surface of metal nanoparticle (or nanostructures)[9]. In order to extend the SERS application to diverse materials and substances, scientists devised various strategies to break the limitation of the substrate generality in the past three decades.[10,11]

In addition of invention of tip-enhanced Raman spectroscopy (TERS) (*vide infra*)[12,13], the core-shell nanoparticle structure seems to be the most effective one. Boosted by the long-range effect of the enhanced electromagnetic field generated by the highly SERS-active Au core, the inherently low- or non-enhancement of the shell material can be substantially boosted to obtain total enhancement factors up to 10^4–10^5.[11] (Fig. S2) With such a high enhancement, one is able to obtain SERS signal of water molecules adsorbed on transition (VIII B group) metals (e.g., Pd, Pt, Rh, Fe, Co, Ni), which were impractical by using the enhancement of SERS of transition metal themselves.[11] However, the strong electromagnetic field will be attenuated exponentially with increasing thickness of the ''spacer'' film, therefore the shell has to be ultra-thin, normally 1-2 nm in thickness. This requirement is hard to meet for many other materials, such as oxides, polymers, insulators or biological membranes, because it is very difficult, if not impossible, to coat them onto Au nanoparticles as uniformly ultra-thin shells at which the probed molecules can adsorb (directly contact with) (Fig. S2). It is therefore highly desirable to explore an innovative approach to make SERS universally applicable.
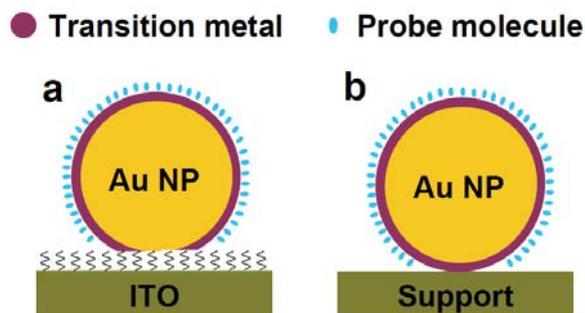
Figure S2 | **Schematic illustration of the contact mode using core-shell NPs.** (a) Coating an ultra-thin transition metal layer on Au nanoparticles dispersed electrodes by the UPD and chemical redox replacement method; (b) synthesizing Au core-transition metal shell nanoparticles by the chemical method.

S3. The advantage of SHINERS over tip-enhanced Raman spectroscopy (TERS)

Since SERS is a nanostructure-based molecular spectroscopy, it is in principle extremely difficult to directly use SERS to study atomically flat single-crystal surfaces that cannot effectively support the strong surface plasmon resonance (SPR). As a consequence, SERS has not been well adopted by the surface science community. There have been only few approaches employing special nanostructures (such as tip-enhanced Raman spectroscopy and ATR configuration) to getting SERS signals from atomically flat single-crystal surfaces (almost all studies were limited in Au(111)) since the mid-1970s.[13-19] TERS combines Raman spectroscopy with scanning probe microscopy by placing a gold tip very close to a single-crystal surface down to 1 nm. As shown in Fig. S3a, by illuminating the nanogap, the localized surface plasmon can be excited at the tip, which will produce a large electromagnetic field enhancement and tremendous increase of the Raman intensity of the molecules adsorbed on the flat surface. An enhancement of 10^6 with highly spatial resolution has been obtained

experimentally, which is allowed to detect adsorbed species on single-crystal surfaces.[13,18,19]
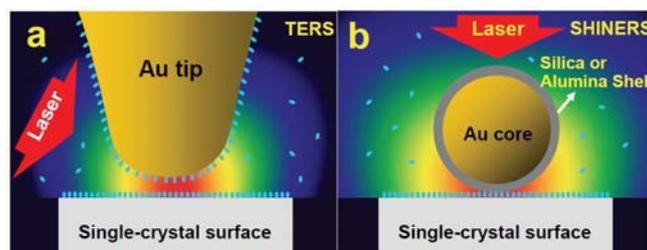
Figure S3 | Schematic illustration of TERS and SHINERS on single-crystal surfaces in solution containing probed molecules. a, TERS as reported in literatures. **b,** SHINERS invented here.

However, such a promising method has not been widely used, e.g., to study single-crystal surfaces (there have been only three papers[13,18,19] on this subject) and not applied in electrochemical environment. It has three drawbacks in comparison with the SHINERS. i) The total intensity contributed by the enhancement is only from one tip. ii) When the Au or Ag tip is approaching to the surface in about 1 nm, the adsorbed molecules may jump up to stick at the bare Au tip. iii) If TERS is applied to electrochemical systems, the tip has to be immersed in the solution, thus any solution species could adsorb at the bare tip. The Raman spectra recorded are dominated by molecules adsorbed at the tip with the highest SERS activity, which may provide misleading information. Moreover, the optical path in solution will be severe distorted for the collection of light scattering. As a consequence, so far TERS has not been able to apply to electrochemical studies. For SHINERS, each Au@SiO$_2$ NP (e.g., diameter = 60 nm) could act as an Au tip in the TERS system (Fig. S3b), and about one thousand "tips" within the laser spot (diameter = 2 μm) can be simultaneously excited,

remarkably increasing the total Raman intensity. More importantly, the Au NP is shelled (protected) with the chemically and electrically inert SiO_2 or Al_2O_3 shell, so the Raman signal is solely from the probed sample (substrate). Therefore, SHINERS can be applied much easily in various materials and environments, especially in solution, which is difficult to realize by TERS for in-situ studying on electrochemical and biologic systems.

S4. Three-dimensional finite-difference time-domain (3D-FDTD) simulation of optical electric-field distribution for SHINERS

In order to understand the mechanism of SHINERS and calculate the field enhancement, a theoretical simulation was carried out by using 3-dimensional finite-difference time-domain (3D-FDTD) method. Figures S4a and b illustrate the calculated optical electric-field distribution on which a 2 × 2 array of Au@SiO_2 NPs is placed on a single-crystal surface of gold. As the Au NPs are brought very close to an atomically flat surface with the controllable spacing by using the glass shell, localized surface plasmons can be excited in the well-controlled nanogap, producing a large electromagnetic field enhancement and a tremendous increase of the Raman intensity for molecules adsorbed on the material's surface beneath the particles, thus allowing the detection of monolayer adsorbed species on a practically important substrate of general interest. The calculated results reveal that the magnitude of the maximally enhanced electric field is about 85 times for the 4 nm shell and about 142 times for the 2 nm shell higher than that of the incident light; and the highest enhancement of Raman scattering appears at the junction between the particle and the substrate as hot spots with ca. 5×10^7 and 4×10^8 fold magnitude respectively. The 3D-FDTD simulation also shows that the

interparticle distance does not affect in any appreciable way on the intensity distribution of electric

field at the particle-substrate region.
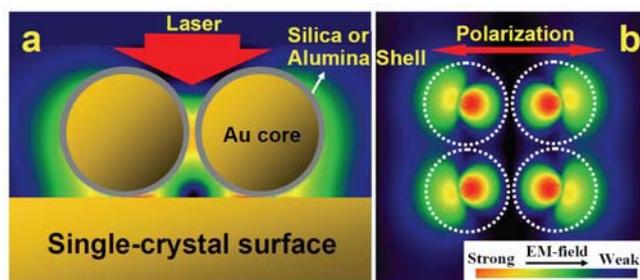
Figure S4 | FDTD simulation of the field-enhancement. The 3D-FDTD simulation of the optical electric field

distribution of a 2×2 array of 55 nm Au@4 nm SiO_2 NPs placed on a single-crystal gold surface. **a,** Side-view and **b,**

Top-view of the optical electric field distribution at the gap between the particle and the surface. The shell-to-shell

distance is 4 nm. The polarization of the 632.8 nm laser is indicated in **b**.

S5. Correlation of the SHINERS intensity and the shell thickness

Since the SPR-based (physical) enhancement of Raman scattering depends critically on the

inter-particle spacing of the nanoparticles (nanostructures), we performed a combined experimental

and theoretical study on the dependence of SHINERS intensity on the silica shell thickness with the

fixed Au core of 55 nm in diameter. The shell thickness was controllably changed from 2 to 20 nm in

sequence, which was confirmed by HRTEM.

Figure S5a presents a set of SHINERS spectra of pyridine (Py) adsorbed on Au@SiO_2 NPs coated

smooth Au substrate. As expected, the SHINERS intensity of Py decreases significantly with the

increasing shell thickness. In other words, the thinner the silica shell, the higher the SHINERS

intensity. To more quantitatively investigate the correlation of the shell thickness and the SHINERS

intensity, we plotted the integrated intensity (normalized with the signal obtained at 2 nm thickness) against the thickness and the result is presented in Fig. S5b as the black square with the error bar. It can be seen that the signal decreases exponentially with the increasing thickness.

We also carried out a 3D-FDTD simulation to the shell thickness dependence using a 2 × 2 array of Au@SiO$_2$ NPs coated at an Au single-crystal surface as the model. Fig. S5 c and d show the optical electric field distribution at the gap between the Au surface and nanoparticles with 2 nm and 8 nm silica shells, respectively. It can be clearly seen that the optical electric field enhancement is considerably higher for the thinner shell (the red color indicates the stronger field). Based on that the surface Raman scattering intensity is enhanced by a factor of approximately proportional to the fourth power of the enhancement of the local incident near field, i.e. $|E_L|^4$,[9] we can correlate the field strength to the SHINERS intensity. Since the field distribution is not uniform (see Fig. S5 c and d), we calculated the averaged SHINERS intensity of the Au(111) coated with Au@SiO$_2$ NPs by integrating the whole sampled area with consideration of the area with different field strength, including the hot spot (red) and other low enhanced field areas (yellow and green). These FDTD data are marked as the red triangle and normalized with the thinnest shell system of 2 nm. The plot shows essentially the same trend as the experimental result as shown in Fig. S5b. Both the experimental and theoretical results confirm that the high sensitivity achieved in SHINERS is attributed to the long-range effect of the enhanced field generated by the encapsulated Au cores.
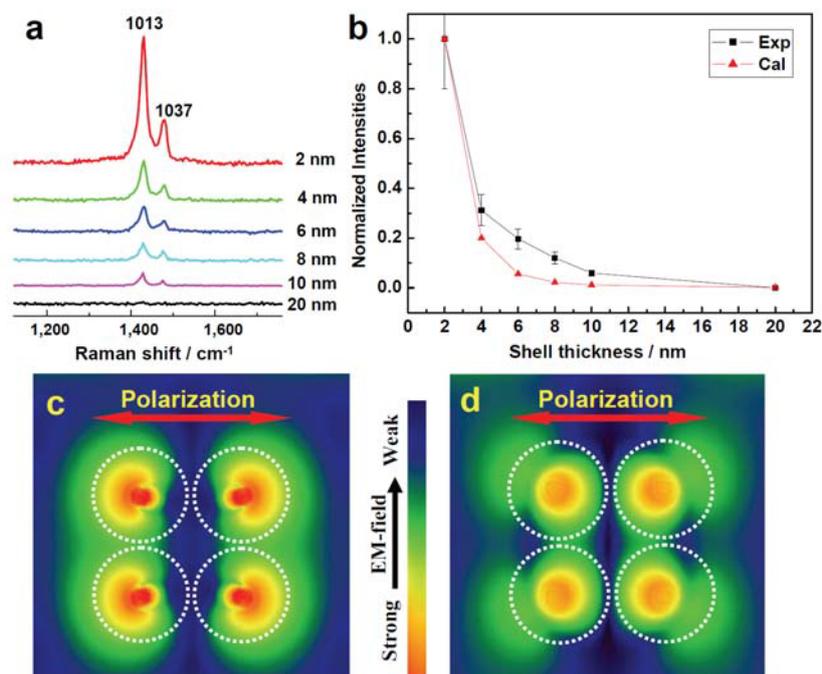
Figure S5 | Shell thickness dependent Raman signal. a, SHINERS spectra of Py adsorbed on a smooth Au surface coated with 55 nm Au@SiO$_2$ NPs with different silica shell thickness. **b,** The shell thickness dependence of the integrated SHINERS intensity of Py (black square) and the corresponding 3D-FDTD calculation result (red triangle). All error bars denote s.e.m. The FDTD simulation of the optical electric field distribution (top-view) at the plane between the single-crystal gold surface and 2 × 2 array of Au@SiO$_2$ with different shell thickness: **c,** 2 nm and **d,** 8 nm.

It should be noted that the "hot-spots" (i.e., the junctions of nanoparticles or nanostructures, at which the intensity magnitude of the electromagnetic field reaches the maximum, and from which the probed molecules emitted the largest Raman photon flux) in the Au@SiO$_2$ NPs used in SHINERS is different from other SERS-active nanostructures. There are two types of "hot-spots" located at the junction of the nanoparticle and the substrate and at the particle-particle junction. For the SHINERS

systems, no probed molecules are hosted in the second type of "hot-spots" because the particles are shelled by inert silica, from which there are no enhanced Raman photons emitted. The SHINERS signal is solely from the probed molecules at the junctions of $Au@SiO_2$ NPs and the substrate.

Regarding the thickness-dependent enhancement factor, our FDTD simulation also indicates that, for 55 nm Au@4 nm SiO_2 nanoparticles, the electric field enhancement factor drops from 85 for the case of 2 × 2 particle matrix to 55 for a single particle case, and the corresponding enhancement of Raman signal drops from 5×10^7 to 9×10^6, which is only a factor of 5.7. Therefore, even for the isolated particle case, the enhancement factor is still rather large. Accordingly, for many applications, it is not necessary to require that the spread nanoparticles being highly ordered or density packed, as long as the spread particles, as the light shiners, are a about monolayer in quantity (the multiple layers will probably block the incident laser light to the probed substrate surface). This is a unique advantage of SHINERS, making it to be used easily.

S6. SHINERS and FTIR spectra of SCN⁻ adsorbed on Au(100) and Au(111)

To examine the capability of SHINERS to distinguish two different single-crystal facets, we have analyzed the spectral features for different single-crystal surfaces of the same metal (Au), using SCN⁻ as the probed molecule. Figures S6 show typically different characters of SCN⁻ adsorbed on Au(100) and Au(111) single-crystal surfaces in high wavenumber region between 2000 cm⁻¹ and 2200 cm⁻¹. First, a sharp peak at around 2119 cm⁻¹, assigned as the C-N stretching mode of SCN⁻, on Au(100) is much stronger than that on Au(111), implying SCN⁻ adsorbed on Au(100) surface mainly through S atom[20-22]. The full width half maximum (FWHM) of the peak for Au(111) is much broader, inferring

that the adsorptions of SCN^- on this facet could through S or N atom[20-22].
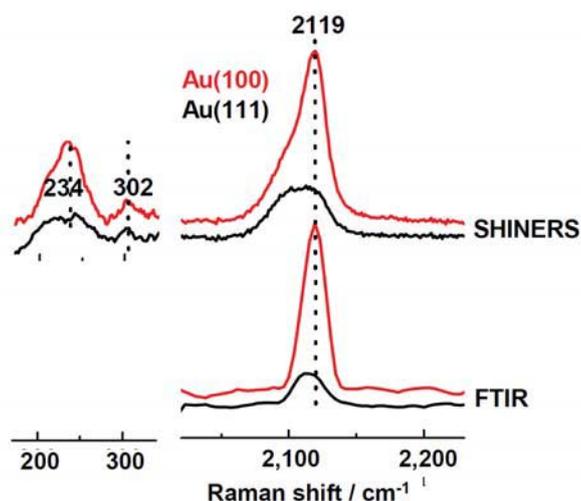
Figure S6 | Comparison of SHINERS with FTIR spectra. SHINERS and FTIR spectra of SCN^- adsorbed on Au(100)

(red lines) and Au(111) (black lines) surfaces in the low and high wavenumber regions at 0.0 V (vs SCE). Solution:

0.01 M NaSCN and 0.1 M $NaClO_4$.

In parallel, we also carried out the experiments using FTIR but with large single-crystal electrodes,

Au(100) and Au(111). In IR results (see Fig. S6), we found that the frequency of ν_{C-N} at 2119 cm^{-1} on

Au(100) is identical to that of SHINERS, and it is a little higher than that on Au(111), and the intensity

on Au(100) is also stronger than that on Au(111). All of these characters are consistent with our

SHINERS experiments.

The slight difference in the band shape between SHINERS and FTIR may originate from the size of

ordered surface domains. In general, the small (100) and (111) facets spontaneously formed on the

single-crystal sphere have larger ordered domains or less surface defects than the corresponding large

single-crystal surfaces obtained from the massive electrode using mechanical cutting.

One of the most important advantages of SHINERS over surface IR spectroscopy is that it can provide direct vibrational information of metal-molecule bonds as shown in the low wavenumber region where two broad peaks at around 234 cm^{-1} and 302 cm^{-1} (see Fig. S6) are assigned as Au-S and Au-N stretching modes, respectively.[20-22] To our knowledge, this is the first Raman spectra representing metal-molecule bonds at two different single-crystal surfaces. It shows that SHINERS may be helpful in unambiguously studying the orientation of adsorbates and for comparing surface selection rules of conventional Raman spectroscopy.

S7. The advantage SHINERS with the isolated mode over SERS with various contact modes

Looking back to the history of SERS, in 1980's the people proposed the "borrowing" idea with depositing metal nanostructures (in the early time those were called micro-islands) directly on a probed surface that is not SERS-active. Van Duyne's group utilized Ag islands on semiconductor surfaces to get SERS from GaAs (1983)[23]; Fleischmann's group (One of the corresponding author of our current paper, Prof. Tian, was the major one who did the experiments) utilized Ni and Co islands on Ag surfaces for SERS (1987)[24]; Devine's group used Ag islands on stainless steel surfaces for SERS (1991)[25]; later, Tian's group demonstrated SERS in an Ag-polymer system (1995)[26]. Since 2002, the synthesis of metal nanoparticles has become routine and several groups have deposited or spread Ag or Au NPs over molecular SAM on smooth Ag or Au surfaces for the SERS study[27,28]. But all previous methods along this direction have three intrinsic problems.

1. *The solution contact.* This problem is similar to TERS as mentioned above. The use of bare

nanoparticles is inapplicable to the liquid (for biology and electrochemistry) or gas (for catalysis)

containing the same probe molecules, other molecules or ions capable of adsorbing on the surfaces of

bare Au nanoparticles (see Fig. S7a). Even in the case of liquid or air containing no such molecules,

the molecules adsorbed on the substrate are likely to diffuse to the probed substrate to bare gold

nanoparticles. The SERS signal generated by the molecules that are adsorbed on the Au nanoparticle

can interfere with or overshadow the SERS signal generated by the molecules adsorbed on the probed

substrate. Since Au nanoparticles are more favorable of SPR than the flat Au or other substrate, the

signal from the nanoparticles is likely to be dominant[9,29,30].
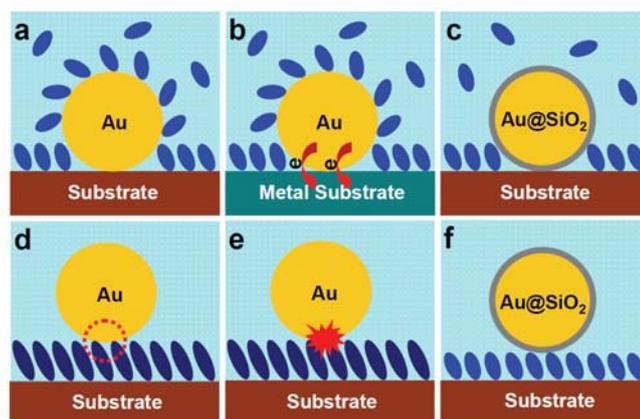
Figure S7 | Schematic illustration of six different surface configurations for SERS or SHINERS measurements.

a-c, In a solution containing probed molecules that can adsorbed at bare Au NPs (**a, b**) but not at the SiO_2 protected Au

NP (**c**). **d-f,** In an air the bare Au NPs (**d, e**) and Au@SiO_2 NP (**f**) are spread over the top of SAM covered substrates.

2. ***The molecule contact***. For studying the self-assembled monolayer (SAM) system. Since the

bottom side of the bare Au nanoparticle is directly in contact with one end of the functional group of

the probe molecules of SAM, such as the amino (NH_2), the thiol (S) or the chlorine (Cl) group (see Fig. S7d), the molecules located between the particles and the substrate are most possibly adopting a two-end adsorption instead of one-end adsorption. This direct contact is likely to change the electron density distribution in the molecule and its adsorption behavior, possibly resulting in a considerable distortion or drastic change in the SERS spectral feature. This will cause a misinterpretation of the recorded data[31]. For some molecular systems, photocatalytic reation could be stimulated owing to a direct contact of the function group of the molecules with the Au nanoparticle, resulting in a change in molecular structure or even new products (Fig. S7e).[32] The PATP example illustrated below is right such an example.

This is illustrated in Fig. S8 where results for four sandwich configurations with *p*-aminothiophenol (PATP) as the probe molecule are directly compared. When bare Au NPs were used, curves I and II show the recorded spectra of PATP adsorbed on flat Au and ZnO nanorods[33,34], the spectra show misleading spectral features due to contact of the amino group of PATP directly to the Au NP itself, which causes the possible photocatalytic dimerization of PATP into an aromatic azo compound as evidenced by the new SERS bands observed at 1139, 1387, and 1433 cm^{-1}.[33,34] Whereas when the same experiment was carried out using Au@SiO$_2$ NPs, curves III and IV, only the spectra for the PATP adsorbed on the Au or ZnO substrate are obtained. Therefore, SHINERS has minimized the interference of the Au NP probe in molecular identification. In the present study, the synthesized Au@SiO$_2$ NPs were carefully studied to ensure that the surface coating is free of pinhole, as can be clearly seen in Fig. 1f, to prevent a direct contact of Au core with the detected molecules or the sample surface (see Supplementary S7).
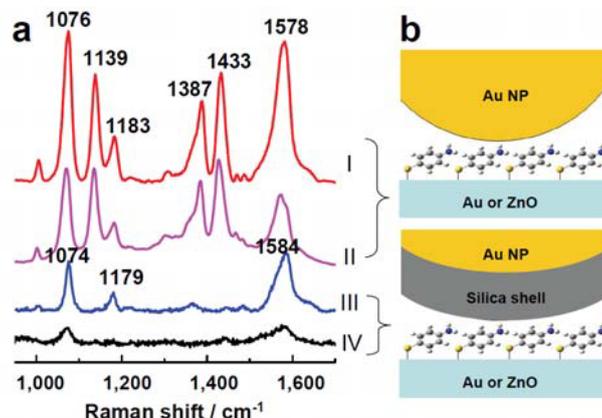
Figure S8 | Comparison of SHIN particles with bare Au NPs on PATP adsorption. a, SERS or SHINERS spectra of

PATP molecules interconnected in different sandwich configurations: (I) Au/PATP/Au NPs, (II) ZnO/PATP/Au NPs, (III)

Au/PATP/Au@SiO$_2$ NPs and (IV) ZnO/PATP/Au@SiO$_2$ NPs.; and the integration acquisition time, was (I) 1 s, (II) 1 s,

(III) 10 s, (IV) 30s; **b,** Schematic illustration of the two different sandwich configurations.

3. ***The electric contact***. If this methodology is extrapolated to non-coinage metals and

semiconductor or to non-SAM molecule systems (see Fig. S7b), the Au nanoparticles could be in

direct contact with the surface of the materials. The difference in the Fermi levels of Au and the

substrate may result in a charge transfer and the creation of a contact potential that, as a consequence,

can significantly affect the electronic structure of the probe molecules located below the Au

nanoparticles[35,36].

Here we used 55 nm Au nanoparticles to probe CO adsorbed at a single crystal Pt(111) surface as an

example. It can be seen from Fig. S9 that there are two strong Raman bands located at 2060 and 2130

cm^{-1}, respectively. The former originates from the stretching vibration of CO adsorbed on Pt, while the

latter is on Au[37] The strong and broad CO band related to the bare Au NPs could mislead the

interpretation about CO adsorption on Pt. More importantly, if we compare the CO(Pt) stretching

frequency in the SERS and SHINERS spectra, we will found it shifts remarkably from 2072 cm^{-1} to

2060 cm^{-1}. This shift is mainly due to the charge transfer (CT) from bare Au NPs to the Pt surface

because the work functions of these two metals are quite different (Au: 5.1 eV, Pt: 5.65 eV in CRC).

This CT will increase the local electron density at the localized Pt surface in contact to Au NPs[35,36],

leading to the large shift of CO stretching frequency. While, SHINERS using shell-isolated Au NPs

can provide correct and meaningful vibrational information regarding the surface adsorbates.
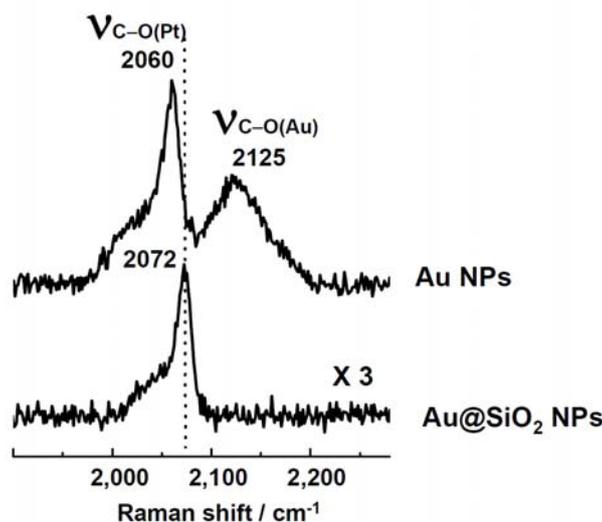
Figure S9 | Comparison of SHIN particles with bare Au NPs on CO adsorption. SERS and SHINERS spectra of

CO adsorbed on a Pt(111) electrode surface, recorded by Au NPs (up) or Au@SiO$_2$ NPs (low) in a solution of 0.1 M

HClO$_4$ saturated by CO gas.

For another SHINERS-SERS comparison experiment, we spread bare or coated Au NPs over a

single crystal Pt(111) surface in a solution under potential control. From Fig. S10, we can clearly see

that the Pt-H frequency recorded using the Au@SiO$_2$ or Au@Al$_2$O$_3$ NPs matches to each other very

well, but the frequency from the bare Au NPs is down-shifted for about 8 cm^{-1} at -1.2 V. This behavior

is similar to the CO system as just mentioned above, which is due to the direct contact of bare Au

nanoparticles with the Pt surface. The charge transfer from Au to Pt may raise the negative charge

density in Pt, resulting in the decrease of the Pt-H stretching frequency[35,36].
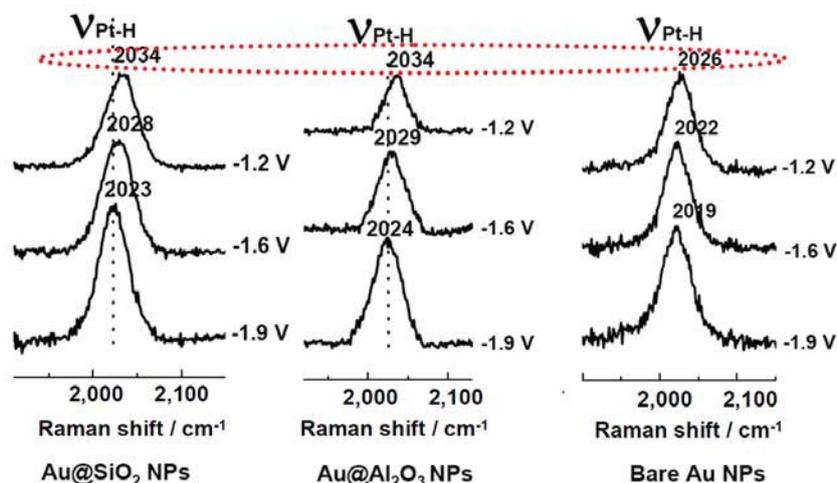
Figure S10 | Comparison of SHIN particles with bare Au NPs on hydrogen adsorption. SHINERS and SERS

spectra of hydrogen adsorption on Pt(111) in a solution of 0.1 M NaClO$_4$ modified by (a) Au@SiO$_2$ NPs, (b)

Au@Al$_2$O$_3$ NPs and (c) bare Au NPs.

SHINERS with its unique isolated mode can overcome the three problems discussed above. By

coating the Au nanoparticles with a thin (chemically and electronically) inert shell, it completely

isolates the Au particles from the probe molecules regardless of whether the measurement is in liquid

or gas phase. Therefore, the measured Raman signal comes from nowhere but the single crystal

sample (other materials) to be measured. The selection of the inert layer has insulated the contact of the Au nanoparticles and the substrate surface, thus, there is no charge transfer, no change in molecular electronic structure and no photocatalysis reaction.

S8. The characterization of pinhole-free from ultra-thin silica shell Au@SiO$_2$ NPs by electrochemical and SERS methods

The most important but difficult part for the SHINERS experiment is how to effectively transfer the strong electromagnetic field from the Au core to the probed objective surface. It is essential to fabricate the Au@SiO$_2$ NPs with an ultra-thin silica shell. However, one must be very cautious on the pinhole effect, because the pinholes of shell will make some tiny areas of the Au core being exposed. In this case, the comparably strong SERS signals from molecules directly adsorbed on the pinhole surfaces may severely interfere with the SERS signal from the molecules adsorbed on the probed substrate, which may then mislead the interpretation of the SERS spectrum. Therefore, to apply the SHINERS strategy to a wide range of materials, the shells must be suitably thin, uniform and ideally free of pinholes unless the probed molecule such as hydrogen that does not adsorb at Au.

To ensure that the synthesized Au@SiO$_2$ core-shell NPs with ultra-thin silica shells are really Au-pinhole-free, we have used cyclic voltammetry (CV) to check it in addition of the HRTEM characterization (Fig. 1f). As shown in Fig. S11, the red curve reveals typical feature of pure 55 nm Au NPs with a characteristic reduction peak at about 0.9 V. On the other hand, the black curve shows the character of 55 nm Au@4 nm SiO$_2$ without the characteristic reduction peak, indicating the Au-pinholes-free character. Furthermore, the ultra-thin silica shells Au@SiO$_2$ NPs have already

displayed very small charging/discharging currents of the electrochemical double layer capacitance,

which also indicates the inert surface chemical property of the thin SiO_2 shell.
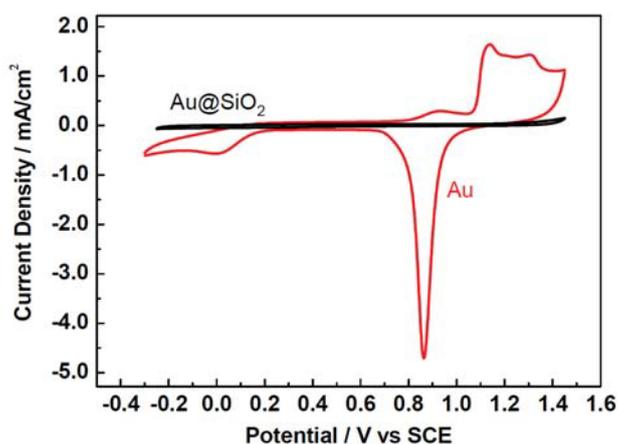
Figure S11 | Electrochemical examination on the pinhole of the shell. Cyclic voltammograms of 55 nm Au (red line)

and 55 nm Au@4 nm SiO_2 (black line) NPs on glassy carbon (GC) electrodes in 0.5 M H_2SO_4 solution. Scan rate: 0.1

V/s.

In addition to the electrochemical examination, we further used a SERS method with pyridine as the

typical probed molecule that is more sensitive to small numbers of pinholes to demonstrate the

pinhole-free character. Firstly, the Au@SiO_2 core-shell NPs were dispersed over a freshly prepared

Au(111) electrode[38]. By controlling the applied potential at −0.6 V, we obtained a strong Raman peak

related to the adsorbed Py on Au (see curve a in Fig. S12). Then we dispersed the 55 nm Au@4 nm

SiO_2 NPs over a smooth Si wafer to which Py has much weak interaction. Just as expected, we did not

observe any signal related to Py for several hours (see curve b). Furthermore, we changed Au@SiO_2

NPs to those with 1 nm shell thickness for the same experiment, and we obtained the strong Raman

signals (curve c) came from Py adsorbed at the Au core through pinholes. All of these experiments

including the HRTEM measurement demonstrate that the Au@SiO$_2$ core-shell NPs with shell

thickness larger than 2 nm are pinhole-free and the SHINERS signals are really from molecules

adsorbed on Pt and Au single-crystal surfaces.
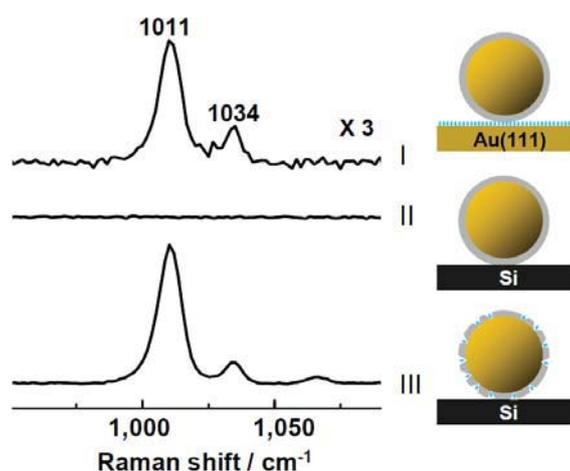
Figure S12 | SERS examination on the pinhole of the shell. SHINERS spectra of Py from 55 nm Au@4 nm SiO$_2$ on

(I) Au(111) and (II) Si wafer, (III) 55 nm Au@1 nm SiO$_2$ NPs with pinholes on Si wafer in 0.01 M Py and 0.1 M

NaClO$_4$ at −0.6 V.

S9. Different strategies of SHINERS from previous SERS works using core-shell structures

Our strategy of using Au@SiO$_2$ NPs is totally different from that of other groups using much

thicker silica shell (generally from 20 to 50 nm)[2-7] or ALD alumina-modified AgFON (silver

film-over-nanosphere)[8,39-41] for the SERS studies. In the cases using the thicker shell, a Raman marker

(preferably molecules with resonant Raman effect) is adsorbed on the very first layer of the

SERS-active Au NP surfaces to produce strong Raman signal of the marker[4-7]. Then the Raman

marker tagged nanoparticles were modified with a thick SiO_2, polyelectrolyte, or polymer shell to provide the mechanical and chemical stability of the tagged molecules and nanoparticles. The shell surface may provide various functional groups for binding with specific molecules for further immunoassay，as exemplified in Fig. S13a. In this configuration, its function is the same as the SiO_2 coated quantum dots, the Raman signal detected is not from the target molecules but from the Raman marker[4-6]. In the case of AgFON@Al_2O_3, a very thin alumina layer (from several angstroms to several nanometers) on AgFON substrates were fabricated by using ALD.[8,39-41] The strategy is to use the alumina layer to stabilize the SERS activity of the underlying Ag film, because Ag is easy to be oxidized and to add the alumina layer for imparting a new chemical functionality to interact (link) with some analytes[8,39-41], as presented in Fig. S13b.

It may be necessary also to note that there are also two types of core-shell nanoparticles widely used in SERS studies. The silica-core-Au-shell NPs shows a great potential in tuning plasmonic structure by simply change the aspect ratio of the Au nanoshell, the ratio of inner to outer radius, and the shell thickness. These nanoparticles can serve as constituents in a new class of materials that are capable of uniquely controlling radiation in the visible and infrared spectral regions. And the Raman enhancement can be designed to follow the plasmon resonance of the individual nanoparticles.[42-44] Au-core-transition-metal-shell NPs has been widely used in electrochemical SERS studies. The inherently low surface enhancement of the transition metals as the shell material can be substantially boosted.[11,45] However, the SERS studies are limited to those molecules that are adsorbed at the Au shell (Fig. S13c) or transition metal shells (Fig. S13d).

Overall, conceptually the strategy of SHINERS is completely different from that of the other four

core-shell nanostructures that have been used for various purposes very successfully[2-8,11,39-45], i.e., the Au-core-silica-shell SERS marker, ALD alumina-modified AgFON, silica-core-Au-shell and Au-core-transition-metal-shell NPs. The Raman signal detected with SHINERS is from the target (probe) molecules adsorbed on the smooth or atomically flat single-crystal surface underneath Au@SiO$_2$ NPs (Fig. S13d), or from the surface components of living cells or other materials. The key feature of SHINERS is that its shell is de-functionalized and chemically inert, simply acting as a spacer and isolator. This makes SHINERS unprecedented applicable for diverse samples and molecules with the large flexibility (see Fig. S13e). However, for SHINERS, we only need to find a way to coat a limited number of materials (such as SiO$_2$, Al$_2$O$_3$ or silicon nitrides) over Au NPs as the isolated shell, then thousands of different materials (substrates) can be studied flexibly.
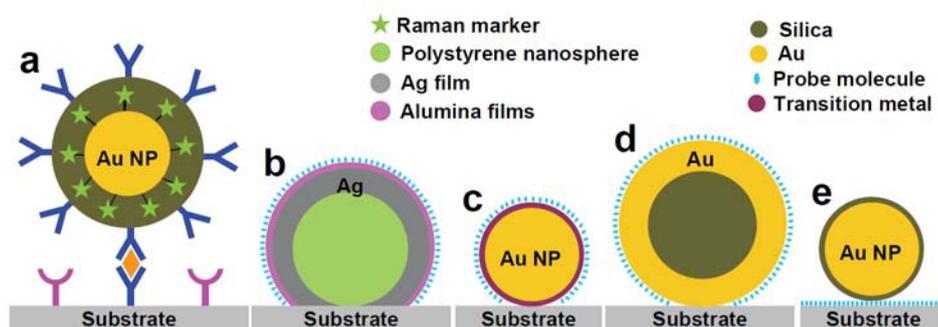
Figure S13 | Schematic illustration of five core-shell NPs with different strategies. a, Au NP coated with thick silica shell with the Raman marker adsorbed directly on the core surface and the inert shell modified with a functional group (in blue) that can bind to the target molecules (in orange). **b,** ALD alumina-modified AgFON substrates stabilize the SERS activity of the underlying silver and detect the analyte adsored at the alumina layer. **c,** Silica-core-Au-shell NPs. **d,** Au-core-transition metal shell NP. **e,** Au NP coated with ultra-thin and chemically inert silica shell.

S10. Inspection of pesticide residues on fruits with portable Raman spectrometer

Given the availability of using portable Raman spectrometer, SHINERS could be applied even widely as a simple-to-use tool for industrial and daily inspection applications. We synthesized another type of SHINs particles, i.e., $Au@SiO_2$ Nanorods, in order to shift the SPR peak to about 770 nm for using 785 nm laser of the portable Raman spectrometer. We spread these nanoparticles as 'shiners' over the probed orange surface and then took the in-situ measurement. The spectra shown in Fig. S14 are the same as in Fig. 4 that were recorded using a confocal Raman microscope. The curve c displays two additional peaks at around 1109 and 1340 cm^{-1}, attributed to the characteristic bands of parathion residues[46]. This preliminary result demonstrates that SHINERS can provide tremendous scope as field-portable and cost-effective analyzer, such as for inspecting food safety, drugs, explosives and environment pollutants accurately and rapidly.
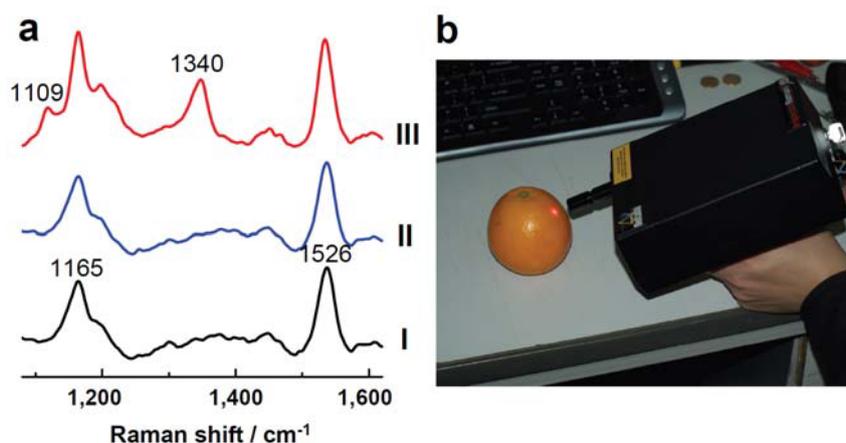
Figure S14 | Inspecting pesticide residues on fruits with portable Raman spectrometer. a, Normal Raman spectra on fresh citrus fruits with (I) clean pericarps and (II) contaminated by parathion. (III) SHINERS spectrum of

contaminated orange modified by rod Au@SiO$_2$ NPs. The excitation line, was 785 nm; laser power on the sample was,

30 mW; and the integration acquisition time, was 30 s. **b,** The picture of the experiment with a portable Raman

spectrometer.

References

S1. Frens, G. Controlled nucleation for regulation of particle-size in monodisperse gold suspension. *Nature Phys. Sci.* **241**, 20-22 (1973).

S2. Liz-Marzán, L. M., Michael, G. & Mulvaney, P. Synthesis of nanosized gold-silica core-shell particles. *Langmuir* **12**, 4329-4335 (1996).

S3. Lu, Y., Yin, Y., Li, Z. Y. & Xia, Y. Synthesis and self-assembly of Au@SiO$_2$ core-shell colloids. *Nano. Lett.* **2**, 785-788 (2002).

S4. Mulvaney, S. P., Musick, M. D., Keating, C. D. & Natan, M. J. Glass-coated, analyte-tagged nanoparticles: A new tagging system based on detection with surface-enhanced Raman scattering. *Langmuir* **19**, 4784-4790 (2003).

S5. Natan, M. J. Concluding remarks surface enhanced Raman scattering. *Faraday Discuss*. **132**, 321-328 (2006).

S6. Smith, W. E. Practical understanding and use of surface enhanced Raman scattering/surface enhanced resonance Raman scattering in chemical and biological analysis. *Chem. Soc. Rev.* **37**, 955-964 (2008).

S7. Doering, W. E. & Nie, S. Spectroscopic tags using dye-embedded nanoparticles and surface-enhanced Raman scattering. *Anal. Chem.* **75**, 6171-6176 (2003).

S8. Zhang, X., Zhao, J., Whitney, A. V., Elam, J. W. & Van Duyne, R. P. Ultrastable substrates for surface-enhanced Raman spectroscopy: Al$_2$O$_3$ overlayers fabricated by atomic layer deposition yield improved anthrax biomarker detection. *J. Am. Chem. Soc.* **128**, 10304-10309 (2006).

S9. Moskovits, M. Surface-enhanced Raman spectroscopy: a brief retrospective. *J. Raman Spectrosc.*

36, 485-496 (2005).

S10. Park, S., Yang, P., Corredor, P. & Weaver, M. J. Transition metal-coated nanoparticle films: vibrational characterization with surface-enhanced Raman scattering. *J. Am. Chem. Soc.* **124**, 2428-2429 (2002).

S11. Tian, Z. Q., Ren, B., Li, J. F. & Yang, Z. L. Expanding generality of surface-enhanced Raman spectroscopy with borrowing SERS activity strategy. *Chem. Comm.* 3514-3534 (2007).

S12. Stöckle, R. M., Suh, Y. D., Deckert, V., Zenobi, R. Nanoscale chemical analysis by tip-enhanced Raman spectroscopy. *Chem. Phys. Lett.* **318**, 131-136 (2000).

S13. Pettinger, B., Ren, B., Picardi, G., Schuster, R. & Ertl, G. Nanoscale probing of adsorbed species by tip-enhanced Raman spectroscopy. *Phys. Rev. Lett.* **92**, 096101-096104 (2004).

S14. Campion, A. & Mullins, D. R. Normal raman scattering from pyridine adsorbed on the low-index faces of silver. *Chem. Phys. Lett.* **94**, 576-579 (1983).

S15. Taylor, C. E., Pemberton, J. E., Goodman, G. G. & Schoenfisch, M. H. Surface enhancement factors for Ag and Au surfaces relative to Pt surfaces for monolayers of thiophenol. *Appl. Spectrosc.* **53**, 1212-1221 (1999).

S16. Bruckbauer, A. & Otto, A. Raman spectroscopy of pyridine adsorbed on single crystal copper electrodes. *J. Raman. Spectrosc.* **29**, 665-672 (1998).

S17. Futamata, M. Highly-sensitive Raman spectroscopy to characterize adsorbates on the electrode. *Surf. Sci.* **386**, 89-92 (1997).

S18. Ren, B., Picardi, G., Pettinger, B., Schuster, R. & Ertl, G. Tip-enhanced Raman spectroscopy of

benzenethiol adsorbed on Au and Pt single-crystal surfaces. *Angew. Chem. Int. Ed.* **44**, 139-142 (2005).

S19. Wang, X., *et al.* Tip-enhanced Raman spectroscopy for investigating adsorbed species on a single-crystal surface using electrochemically prepared Au tips. *Appl. Phys. Lett.* **91**, 101105 (2007).

S20. Li, X. & Gewirth, A. A. Potential-dependent reorientation of thiocyanate on Au electrodes. *J. Am. Chem. Soc.* **125**, 11674-11683 (2003).

S21. Gao, P. & Weaver, M. J. Metal-adsorbate vibrational frequencies as a probe of surface bonding: halides and pseudohalides at gold electrodes. *J. Phys. Chem.* **90**, 4057-4063 (1986).

S22. Corrigan, D. S., Foley, J. K., Gao, P., Pons, S. & Weaver, M. J. Comparisons between surface-enhanced Raman and surface infrared spectroscopies for strongly perturbed adsorbates: thiocyanate at gold electrodes. *Langmuir* **1**, 616-620 (1985)

S23. Van Duyne, R. P. & Haushalter, J. P. Surface-enhanced Raman spectroscopy of adsorbates on semiconductor electrode surfaces: tris(bipyridine)ruthenium(II) adsorbed on silver-modified n-gallium arsenide(100). *J. Phys. Chem.* **87**, 2999-3003 (1983).

S24. Fleischmann, M. & Tian, Z. Q. The induction of SERS on smooth Ag by the deposition of Ni and Co. *J. Electroanal. Chem.* **217**, 411-416 (1987).

S25. Gui, J. & Devine, T. M. Obtaining surface-enhanced Raman spectra from the passive film on iron. *J. Electrochem. Soc.* **138**, 1376-1384 (1991).

S26. Gao, J. S., Chen, Y. X. & Tian, Z. Q. SERS effect induced from conducting polymer/solution interfaces. *Chin. J. Electrochemistry* **1**, 141-145 (1995).

S27. Zheng, J. *et al.* Surface-enhanced Raman scattering of 4-Aminothiophenol in assemblies of nanosized particles and the macroscopic surface of silver. *Langmuir* **19**, 632-636 (2003).

S28. Ikeda, K., Fujimoto, N., Uehara, H. & Uosaki, K. Raman scattering of aryl isocyanide monolayers on atomically flat Au(111) single crystal surfaces enhanced by gap-mode plasmon excitation. *Chem. Phys. Lett.* **460**, 205-208 (2008).

S29. Mullins, D. R. & Campion, A. Unenhanced Raman scattering from pyridine chemisorbed on a stepped silver surface: Implications for proposed sers mechanisms. *Chem. Phys. Lett.* **110**, 565-570 (1984).

S30. Gersten, J. & Nitzan, A. Electromagnetic theory of enhanced Raman scattering by molecules adsorbed on rough surfaces. *J. Chem. Phys.* **73**, 3023-3037 (1980).

S31. Jaiswal, A., Tavakoli, K. G. & Zou, S. Electromagnetic theory of enhanced Raman scattering by molecules adsorbed on rough surfaces. *Anal. Chem.* **78**, 120-124 (2006).

S32. Bond, G. C., David, C. L. & Thompson, T. *Catalysis by Gold.* (Imperial College Press, London, 2006.)

S33. Grirrane, A., Corma, A. & Garcia, H. Gold-catalyzed synthesis of aromatic azo compounds from anilines and nitroaromatics. *Science*, **322**, 1661-1664 (2008).

S34. Wu, D. Y. *et al.* Surface catalytic coupling reaction of p-mercaptoaniline linking to silver nanostructres responsible fro abnormal SERS enhancement: a DFT study. *J. Phys. Chem. C* **113**, 18212-18222(2009).

S35. Rodriguez, J. A. & Goodman, D. W. The nature of the metal-metal bond in bimetallic surfaces. *Science* **257**, 897-903 (1992).

S36. Zhang, J., Sasaki, K., Sutter, E. & Adzic, R. R. Stabilization of Platinum oxygen-reduction electrocatalysts using gold clusters. *Sicence* **315**, 220-222 (2007).

S37. Zou, S. & Weaver, M. J. Surface-enhanced Raman scattering on uniform transition-metal films: toward a versatile adsorbate vibrational strategy for solid-nonvacuum interfaces? *Anal. Chem.* **70**, 2387-2395 (1998).

S38. Clavilier, J., Armand, D., Sun, S. G. & Petit, M. Electrochemical adsorption behaviour of platinum stepped surfaces in sulphuric acid solutions. *J. Electroanal. Chem.* **205**, 267-277 (1986).

S39. Stiles, P. L., Dieringer, J. A., Shah, N. C. & Van Duyne, R. P. Surface-enhanced Raman spectroscopy. *Annu. Rev. Anal. Chem.* **1**, 601-626 (2008).

S40. Whitney, A. V. *et al.* Localized surface plasmon resonance nanosensor: a high-resolution distance-dependence study using atomic layer deposition. *J. Phys. Chem. B* **109**, 20522-20528 (2005).

S41. Dieringer, J. A. *et al.* Surface enhanced Raman spectroscopy: new materials, concepts, characterization tools, and applications. *Faraday Discuss*. **132**, 9-26 (2006).

S42. Oldenburg, S. J., Averitt, R. D., Westcott, S. L. & Halas, N. J. Nanoengineering of optical resonances. *Chem. Phys. Lett.* **288**, 243-247 (1998).

S43. West, J. L. & Halas, N. J. Engineered nanomaterials for biophotonics applications: improving sensing, imaging, and therapeutics. *Annu. Rev. Biomed. Eng.* **5**, 285-292 (2003).

S44. Jackson, J. B., Westcott, S. L. & Hirsch, L. R. Controlling the surface enhanced Raman effect via the nanoshell geometry. *Appl. Phys. Lett.* **82**, 257-259 (2003).

S45. Wu, D. Y., Li, J. F., Ren, B. & Tian, Z. Q. Electrochemical surface-enhanced Raman spectroscopy of nanostructures. *Chem. Soc. Rev.* **37**, 1025-1041 (2008).

S46. Lee, D. *et al.* Quantitative analysis of methyl parathion pesticides in a polydimethylsiloxane microfluidic channel using confocal surface-enhanced Raman spectroscopy. *Appl. Spectrosc.* **60,** 373-377 (2006).